J. Fluid Mech. (2022), *vol*. 951, R3, doi:10.1017/jfm.2022.902

Weakly nonlinear evolution of stochastically driven non-normal systems

Yves-Marie Ducimetière[1],†, **Edouard Boujo**[1] **and François Gallaire**[1]

[1]Laboratory of Fluid Mechanics and Instabilities, EPFL, 1015 Lausanne, Switzerland

(Received 1 July 2022; revised 29 August 2022; accepted 20 October 2022)

We consider nonlinear dynamical systems driven by stochastic forcing. It has been largely evidenced in the literature that the linear response of non-normal systems (e.g. fluid flows) may exhibit a large variance amplification, even in a linearly stable regime. This linear response, however, is relevant only in the limit of vanishing forcing intensity. As the intensity increases, the frequency distribution and the variance of the response may be strongly modified due to nonlinear effects. To go beyond this limitation, we propose a theoretical approach to derive an amplitude equation governing the weakly nonlinear evolution of these systems. This approach does not rely on the presence of an eigenvalue close to the neutral axis, applying instead to any sufficiently non-normal operator, and the Fourier components of the response are allowed to be arbitrarily different from any eigenmode. The methodology is outlined for a generic nonlinear dynamical system, and the application case highlights a common non-normal mechanism in hydrodynamics: convective non-normal amplification in the flow past a backward-facing step.

Key words: instability, nonlinear dynamical systems

1. Introduction

Some flows experience transition from laminar to turbulent far below the threshold predicted by linear stability theory, which relies on the eigenvalues of the linearised Navier–Stokes operator. In addition, the value of the bifurcation parameter at the transition strongly depends on the level of external noise. Among them are the canonical Couette and Poiseuille parallel shear flows, as detailed in Schmid & Henningson (2001). Non-parallel flows such as jets and the backward-facing step (BFS) flow, studied for instance in Garnaud *et al.* (2013) and Blackburn, Barkley & Sherwin (2008), should also be mentioned.

† Email address for correspondence: yves-marie.ducimetiere@epfl.ch

The transition scenario advanced in Trefethen *et al.* (1993) relies on the *non-normality* property of the linearised Navier–Stokes operator. The latter implies that a linearly stable flow can nevertheless strongly amplify a small initial structure or a sustained forcing term through non-modal mechanisms (see Schmid (2007) for a review). Thereby, the response may be carried into a regime where nonlinearities set in and the flow escapes from its linearly stable solution.

In this perspective, numerous studies have computed the small-amplitude structures that are the *most amplified* by the flow: initial conditions, harmonic forcing or stochastic forcing, resulting, respectively, in optimal transient growth, harmonic gain and stochastic gain. Formally, such studies generally consist in finding the singular mode of a specific linear operator, which can be very different from the eigenmodes of the linearised Navier–Stokes operator. For the harmonic forcing problem, one could for instance refer to the work of Schmid & Henningson (2001) and Jovanović & Bamieh (2005) on the parallel plane Couette and Poiseuille flows. The problem of the flow response to a stochastic forcing, studied in the rest of this paper, mimics more realistic situations. Indeed, unpredictable noise may arise from different sources in Nature, such as residual turbulence, variation of atmospheric conditions, acoustic disturbances, geometrical defects and many others. The response to white noise has, for instance, been considered for the plane Couette and Poiseuille flows in Farrell & Ioannou (1993), and in Dergham, Sipp & Robinet (2013) for the BFS flow. Owing to the non-normality of the linearised operator, all these flows can sustain a large variance even if the noise intensity is comparatively weak.

In the linear paradigm, however, amplifications do not depend on the amplitude of the initial condition or forcing. The latter are assumed arbitrarily small, such that nonlinear terms are negligible. Therefore, the nonlinear interactions involved in the subcritical transition or in the saturation process cannot be captured by definition. For this reason, more elaborate models accounting for a nonlinear coupling between the mean flow and the linear perturbation have been proposed. For instance, Marston, Conover & Schneider (2008) considered a barotropic flow on a rotating sphere, and performed a cumulant expansion of the vorticity statistics that was closed by neglecting the third and higher cumulants; this amounts to neglecting the fluctuation–fluctuation interactions while retaining the fluctuation–mean flow interactions. By comparison with statistics accumulated directly in direct numerical simulations (DNS), Marston *et al.* (2008) showed that this truncation was well justified in certain regimes (see their figures 5 and 6), for instance when the relaxation time towards a zonal jet was short, in which case the fluctuations were suppressed by the strong coupling to the jet.

Instead of being neglected, the fluctuation–fluctuation interactions are sometimes replaced by a stochastic parametrisation, for instance white noise, as originally done in Farrell & Ioannou (2003). This led to the stochastic structural stability theory (S3T or SSST), which was, for instance, able to describe sustained coherent structures appearing during the transition to turbulence in two-dimensional atmospheric flows, as well as in three-dimensional parallel Couette flow (Farrell & Ioannou 2012). In these shear flows, the success of the SSST theory, despite the fact that modelling the fluctuation–fluctuation interactions as white noise seems to be an oversimplification, is explained as follows in Farrel & Ioannou (2019):

> In the case of homogeneous isotropic turbulence the stochastic excitation must be very carefully fashioned in order to obtain approximately valid statistics using a stochastic closure [...] while in shear flow the form of the stochastic excitation is not crucial. The reason is that in shear flow the [Navier–Stokes] operator [linearized around the mean flow] is non-normal and a restricted set of perturbations participate strongly in the interaction with the mean flow. As a result the statistical

> state of the turbulence is primarily determined by the quasilinear interaction between the mean and these perturbations rather than by nonlinear interaction among the perturbations.

This 'quasi-linear' approach, which consists in allowing fluctuation–mean flow interactions and either neglecting or modelling other interactions, has been extended to a resolvent-based approach applied to a turbulent pipe flow in McKeon & Sharma (2010). The Navier–Stokes equations (NSE) were reformulated as a nonlinear equation for the mean velocity, and an input–output equation for the fluctuation, where the latter is the linear response to a forcing term modelling the nonlinear fluctuating term through the resolvent operator around the mean velocity. The closure problem for the mean flow equation is avoided by knowing *a priori* the mean profile from experimental data. Following an argument essentially similar to the one quoted above from Farrel & Ioannou (2019), when the resolvent operator is low-rank, in the sense that there exists a small set of forcing–response pairs of modes associated with gains much larger than all the others, the fluctuation can be well approximated as a combination of these leading response modes.

This type of mean flow–resolvent analysis has been performed by numerous authors since then, and has often proven successful in reproducing the main features of self-sustained turbulence. This was the case for the turbulent jet studied in Pickering *et al.* (2020), where the resolvent mode around a mean-flow eddy-viscosity model projected well on the spectral proper orthogonal decomposition (SPOD) modes that optimally describe the turbulent flow statistics from large-eddy simulation (LES) data. Note that, because of the non-normality of the resolvent operator, strong amplification may occur even in the absence of a dominant eigenvalue in the (eigen)spectrum of the linearised Navier–Stokes operator around the mean flow; for this reason the question of the relevance of a stability analysis around the mean flow is discussed in Symon *et al.* (2018). Recently, a resolvent-based approach was also adopted in Rosenberg & McKeon (2019) to compute travelling waves in Couette and Poiseuille flow. Instead of assuming the mean flow to be known *a priori*, the coupled system was solved iteratively, requiring only the knowledge of the travelling wave speed and amplitude.

The quasi-linear assumption that the dominant nonlinear mechanism is the Reynolds stress feedback onto the mean flow excludes, for instance, systems with strong harmonic generation and subharmonic excitation, as illustrated in Meliga (2017). It has also proven to be in default in Tobias & Marston (2013) in the case of turbulent zonal jets that are driven too far from equilibrium (for which the rates of forcing and dissipation go to zero). A generalisation has been proposed in Marston, Chini & Tobias (2016), leading to a system constituted of a nonlinear equation for the slowly varying part of the velocity field (instead of just the mean flow), and a linear equation for the rapidly varying part (instead of the entire fluctuations); in this manner, the small scales can exchange energy with each other, through their interaction with the large scales. With a sufficiently large number of modes included in the slowly varying part, this generalised model converges and improves the predictions, at increased numerical cost.

Amplitude equations for the response of nonlinear systems to stochastic forcing constitute another class of modelling techniques, in principle restricted to the weakly nonlinear regime, but much cheaper to implement. The technique was developed for instance in Rajan & Davies (1988) and Nayfeh & Serhan (1990) using the method of multiple scales and/or stochastic averaging on the Duffing and Duffing–Rayleigh oscillators, respectively. Similar to their deterministic counterparts, however, the possibility to construct these simplified equations relies on the existence of a resonant frequency, as they describe the slowly varying modulation of the associated eigenmode.

In our previous work (Ducimetière, Boujo & Gallaire 2022), we derived an amplitude equation to prolong the linear harmonic gain (and transient growth) curve in a weakly nonlinear regime by increasing the forcing amplitude. The method does not rely on modal quantities, in contrast to classical techniques, and the present paper aims at generalising this method to the response to stochastic forcing. Namely, we derive an equation for the weakly nonlinear evolution of the optimal linear response. Here, no assumptions are made on the dominant nonlinear interaction mechanisms, and the Fourier (frequency) components of the linear response can be arbitrarily different from eigenmodes as long as the linear operator is sufficiently non-normal. The amplitude equation is written directly in the Fourier domain, and depends solely on the frequency. Thereby, the weakly nonlinear evolution of the flow response to stochastic forcing can be determined at a numerical cost considerably lower than that of a DNS, since (i) it is independent of the number of spatial degrees of freedom, and (ii) it does not require a long simulated time to reach statistical convergence.

2. Linear regime

A generic nonlinear dynamical system is considered,

$$\partial_t \boldsymbol{U} = N(\boldsymbol{U}) + \boldsymbol{F}, \tag{2.1}$$

where $N(\cdot)$ is a nonlinear operator and $\boldsymbol{F}$ a forcing term. The first step of our analysis is to linearise (2.1) around an unforced equilibrium $\boldsymbol{U}_e$ solution of $N(\boldsymbol{U}_e) = \boldsymbol{0}$. Small-amplitude forcing and perturbations, $\epsilon \boldsymbol{f}$ and $\epsilon \boldsymbol{u}$ ($\epsilon \ll 1$), are considered around $\boldsymbol{U}_e$. An asymptotic expansion of (2.1) in terms of ϵ can thus be performed. At order ϵ, the fields $\boldsymbol{u}$ and $\boldsymbol{f}$ are linked through the linear relation

$$\partial_t \boldsymbol{u} = \boldsymbol{L}\boldsymbol{u} + \boldsymbol{f}, \tag{2.2}$$

where L results from the linearisation of N around $\boldsymbol{U}_e$.

For fluid flows governed by the incompressible NSE, $\boldsymbol{L}\boldsymbol{u} = -(\boldsymbol{U}_e \cdot \boldsymbol{\nabla})\boldsymbol{u} - (\boldsymbol{u} \cdot \boldsymbol{\nabla})\boldsymbol{U}_e + Re^{-1}\Delta \boldsymbol{u} - \boldsymbol{\nabla} p(\boldsymbol{u})$, where Re is the Reynolds number, and where the pressure field p is such that the velocity field $\boldsymbol{u}$ is divergence-free. Note that both fields are linked through a linear Poisson equation. In practice, p is included in the state variable, resulting in a singular mass matrix, omitted here for the sake of clarity.

The specific form $\boldsymbol{f}(\boldsymbol{x}, t) = \boldsymbol{f}_s(\boldsymbol{x})\xi(t)$ is chosen for the stochastic forcing, where $\boldsymbol{f}_s(\boldsymbol{x})$ is the forcing spatial structure and $\xi(t)$ is a δ-correlated white noise process with zero mean, i.e.

$$\langle \xi(t) \rangle = 0, \quad \langle \xi(t)\xi(t-b)^* \rangle = \delta(b), \tag{2.3a,b}$$

where $\langle \cdot \rangle$ denotes ensemble averaging and the superscript $*$ denotes complex conjugation. The process $\xi(t)$ is the only source of randomness of the system. We introduce the Fourier transform $\mathcal{F}[\cdot]$ of a temporal signal of length $[0, T]$ with $T \to \infty$, and its inverse $\mathcal{F}^{-1}[\cdot]$ as

$$\hat{\boldsymbol{u}}(\omega) = \mathcal{F}[\boldsymbol{u}(t)] = \frac{1}{\sqrt{T}} \int_0^T \boldsymbol{u}(t) \mathrm{e}^{-\mathrm{i}\omega t} \, \mathrm{d}t, \quad \boldsymbol{u}(t) = \mathcal{F}^{-1}[\hat{\boldsymbol{u}}(\omega)] = \frac{\sqrt{T}}{2\pi} \int_{-\infty}^{\infty} \hat{\boldsymbol{u}}(\omega) \mathrm{e}^{\mathrm{i}\omega t} \, \mathrm{d}\omega. \tag{2.4a,b}$$

We verify that $\boldsymbol{u}(t) = \mathcal{F}^{-1}[\mathcal{F}[\boldsymbol{u}(t)]]$ using the definition of a Dirac impulse $2\pi\delta(t) = \int_{-\infty}^{\infty} \mathrm{e}^{\mathrm{i}\omega t} \, \mathrm{d}\omega$, and its property $\int_0^T \boldsymbol{u}(s)\delta(t) \, \mathrm{d}s = \boldsymbol{u}(t)$.

In the statistically steady regime, (2.2) can be solved in the Fourier domain as $\hat{\boldsymbol{u}}(\omega) = \hat{\xi}(\omega)R(\omega)\boldsymbol{f}_s$, where

$$R(\omega) \doteq (\mathrm{i}\omega I - L)^{-1} \tag{2.5}$$

is the resolvent operator. It follows from (2.3*a*,*b*) that $\langle\hat{\xi}(\omega)\hat{\xi}(\omega+b)^*\rangle = \int_0^T \mathrm{e}^{\mathrm{i}tb}\,\mathrm{d}t/T = 2\pi\delta(b)/T$; in addition, using that $|\hat{\xi}(\omega)|^2 = \int_0^T T^{-1}\int_0^T \xi(t)\xi(t-b)\,\mathrm{d}t\,\mathrm{e}^{-\mathrm{i}\omega b}\,\mathrm{d}b$ and that $\xi(t)$ is a stationary and ergodic process, it turns out that $|\hat{\xi}(\omega)|^2 = 1$. Namely, $\hat{\xi}(\omega)$ has random phases uniformly distributed between 0 and 2π, but a deterministic unit amplitude for all frequencies.

As considered in Farrell & Ioannou (1993) a relevant measure of input–output gain of the system (2.2) is the ratio of the statistically steady variance maintained by the stochastic forcing, $\langle||\boldsymbol{u}(t)||^2\rangle$, over the energy spectral density of the forcing $1||\boldsymbol{f}_s||^2$. The variance of the response is *not* compared with the variance of the stochastic forcing, as $\langle\xi(t)^2\rangle$ diverges by definition (2.3*a*,*b*) of the white noise. Optimising over the forcing structure, the maximum attainable gain is

$$G = \max_{\boldsymbol{f}_s}\frac{\langle||\boldsymbol{u}(t)||^2\rangle}{||\boldsymbol{f}_s||^2} \doteq \frac{1}{\epsilon_o^2}. \tag{2.6}$$

In the following, we choose for $||\cdot||$ the L^2 norm induced by the Hermitian inner product $\{\hat{\boldsymbol{u}}_a, \hat{\boldsymbol{u}}_b\} = \int_\Omega \hat{\boldsymbol{u}}_a^{\mathrm{H}}\hat{\boldsymbol{u}}_b\,\mathrm{d}\Omega$ (the superscript H denotes the Hermitian transpose). The operator $R(\omega)^\dagger$ denotes the adjoint of $R(\omega)$ under this scalar product, such that $\{R(\omega)\hat{\boldsymbol{u}}_a, \hat{\boldsymbol{u}}_b\} = \{\hat{\boldsymbol{u}}_a, R(\omega)^\dagger\hat{\boldsymbol{u}}_b\}$ for any $\hat{\boldsymbol{u}}_a$ and $\hat{\boldsymbol{u}}_b$. Using the inverse Fourier transform of $\boldsymbol{u}(t)$, we can write (Farrell & Ioannou 1996)

$$\langle||\boldsymbol{u}(t)||^2\rangle = \int_\Omega \boldsymbol{f}_s^{\mathrm{H}}B^\infty\boldsymbol{f}_s\,\mathrm{d}\Omega = \{\boldsymbol{f}_s, B^\infty\boldsymbol{f}_s\}, \quad \text{with } B^\infty = \frac{1}{2\pi}\int_{-\infty}^{\infty} R(\omega)^\dagger R(\omega)\,\mathrm{d}\omega. \tag{2.7}$$

The operator B^∞ is a positive definite Hermitian with positive and real eigenvalues associated with mutually orthogonal eigenvectors. The maximum gain (2.6) is the largest eigenvalue of B^∞. The associated eigenvector, denoted $\boldsymbol{f}_o$ and normalised as $\{\boldsymbol{f}_o, \boldsymbol{f}_o\} = ||\boldsymbol{f}_o||^2 = 1$, is the optimal forcing structure (hence the subscript 'o'), i.e the forcing structure that leads to the largest stochastically maintained variance. If in addition the largest eigenvalue of B^∞ is much larger than all the others, which correspond to suboptimal gains, and if the actual (unknown) forcing of the system does not trigger a particular suboptimal eigenvector of B^∞ but projects comparably on all the eigenvectors, then the response to the actual forcing is expected to be dominated by the response to the optimal forcing $\boldsymbol{f}_o$, regardless of the specific shape of the actual forcing.

This low-rank approximation is commonly done and well justified for strongly non-normal operators (Symon *et al.* 2018), and explains why we restrict our analysis to the response to $\xi(t)\boldsymbol{f}_o$ and do not include additional forcing modes. By linearity, forcing the system (2.2) with $\boldsymbol{f} = \epsilon_o\xi(t)\boldsymbol{f}_o$, where we define $\epsilon_o^2 \doteq 1/G$, leads to a response $\boldsymbol{l}(t)$ of unit variance, $\langle||\boldsymbol{l}(t)||^2\rangle = \epsilon_o^2\{\boldsymbol{f}_o, B^\infty\boldsymbol{f}_o\} = 1$, and zero mean, $\langle\boldsymbol{l}(t)\rangle = 0$. In the Fourier domain, $\hat{\boldsymbol{l}}(\omega) = \epsilon_o\hat{\xi}(\omega)R(\omega)\boldsymbol{f}_o = \hat{\xi}(\omega)\hat{\boldsymbol{q}}(\omega)$, where we have introduced the *deterministic* field $\hat{\boldsymbol{q}}(\omega) \doteq \epsilon_o R(\omega)\boldsymbol{f}_o$, or

$$R(\omega)^{-1}\hat{\boldsymbol{q}}(\omega) = \epsilon_o\boldsymbol{f}_o. \tag{2.8}$$

Since L is strongly non-normal, as assumed in the rest of the present study, neither of ϵ_o or $\boldsymbol{f}_o$ are immediately determined from its spectral (modal) properties; furthermore, strong

non-normality implies $\epsilon_o \ll 1$ (Farrell & Ioannou 1993). It follows from (2.8) that we can perturb the inverse resolvent as

$$\Phi(\omega) \doteq R(\omega)^{-1} - \epsilon_o P(\omega), \quad \text{where } P(\omega) = \boldsymbol{f}_o \frac{\{\hat{\boldsymbol{q}}(\omega), \cdot\}}{||\hat{\boldsymbol{q}}(\omega)||^2}, \tag{2.9}$$

i.e. the linear operator $P(\omega)$ is such that $P(\omega)\hat{\boldsymbol{g}}(\omega) = \boldsymbol{f}_o\{\hat{\boldsymbol{q}}(\omega), \hat{\boldsymbol{g}}(\omega)\}||\hat{\boldsymbol{q}}(\omega)||^{-2}$, for any field $\hat{\boldsymbol{g}}(\omega)$. This leads to $\Phi(\omega)\hat{\boldsymbol{q}}(\omega) = \boldsymbol{0}$, for all ω, such that $\Phi(\omega)$ is a singular operator for each frequency and $\hat{\boldsymbol{q}}(\omega)$ its non-trivial kernel.

Expansion (2.9) is justified *a priori* only over the range of frequencies for which $||R(\omega)^{-1}|| \gg \epsilon_o||P(\omega)|| = ||R(\omega)\boldsymbol{f}_o||^{-1}$, where we have used that $||P(\omega)|| = ||\hat{\boldsymbol{q}}(\omega)||^{-1}$. Since $||R(\omega)^{-1}||$ is equal to the inverse of the smallest singular value of $R(\omega)^{-1}$, the latter inequality can be re-expressed as $||R(\omega)\boldsymbol{f}_o|| \gg \min_{||\boldsymbol{f}||=1} ||R(\omega)\boldsymbol{f}||$. In other words, the expansion is justified for all frequencies that amplify the optimal forcing structure $\boldsymbol{f}_o$ much more than the least amplified structure, which can be seen as a condition of large 'spectral' gap in the singular values. Note that both $P(\omega)$ and $\Phi(\omega)$ are deterministic operators. Using that $P(\omega)^\dagger = \hat{\boldsymbol{q}}(\omega)\{\boldsymbol{f}_o, \cdot\}/||\hat{\boldsymbol{q}}(\omega)||^2$, we can show that the non-trivial kernel of the adjoint operator $\Phi(\omega)^\dagger$ is $\hat{\boldsymbol{a}}(\omega) \doteq R(\omega)^\dagger\hat{\boldsymbol{q}}(\omega)$, i.e. $\Phi(\omega)^\dagger\hat{\boldsymbol{a}}(\omega) = \boldsymbol{0}$.

3. Weakly nonlinear regime

We now develop a method to derive an amplitude equation for the weakly nonlinear amplification of a stochastic forcing.

3.1. *Generic nonlinear system and application to a toy model*

The method is based on a multiple-scale asymptotic expansion, for which the gain inverse $\epsilon_o \ll 1$ constitutes a natural choice of small parameter. The system (2.1) is weakly forced by $\boldsymbol{F} = \phi\epsilon_o^2\boldsymbol{f}_h\xi(t)$. In general, the spatial forcing structure $\boldsymbol{f}_h$ need not be chosen as the optimal one $\boldsymbol{f}_o$. We impose $||\boldsymbol{f}_h||^2 = 1$ such that the prefactor $\phi = O(1)$ sets the forcing amplitude $F \doteq ||\phi\epsilon_o^2\boldsymbol{f}_h|| = \phi\epsilon_o^2$. A separation of time scales is assumed for the response, with the slow time scale $\tau_1 \doteq \epsilon_o t$ aiming at capturing slow variations of the response

$$\boldsymbol{U}(t, \tau_1) = \boldsymbol{U}_e + \epsilon_o\boldsymbol{u}_1(t, \tau_1) + \epsilon_o^2\boldsymbol{u}_2(t, \tau_1) + O(\epsilon_o^3) \tag{3.1}$$

around the statistically steady regime.

Introducing the expansion (3.1) into (2.1), isolating the Fourier component at ω and perturbing $R(\omega)^{-1}$ according to (2.9) yields

$$\epsilon_o[\Phi\hat{\boldsymbol{u}}_1] + \epsilon_o^2[\Phi\hat{\boldsymbol{u}}_2 + \mathrm{d}_{\tau_1}\hat{\boldsymbol{u}}_1 - \mathcal{F}[N_2(\boldsymbol{u}_1)] - \phi\boldsymbol{f}_h\hat{\xi} + P\hat{\boldsymbol{u}}_1] + O(\epsilon_o^3) = \boldsymbol{0}, \tag{3.2}$$

where $N(\boldsymbol{U}) = N(\boldsymbol{U}_e) + \epsilon_o L\boldsymbol{u}_1 + \epsilon_o^2[L\boldsymbol{u}_2 + N_2(\boldsymbol{u}_1)] + O(\epsilon_o^3)$, and $\hat{\boldsymbol{u}}_i = \hat{\boldsymbol{u}}_i(\tau_1; \omega)$ for $i = 1, 2$. At order $O(\epsilon_o)$ of the expansion (3.2), we obtain $\Phi(\omega)\hat{\boldsymbol{u}}_1(\tau_1; \omega) = \boldsymbol{0}$. Since by construction $\hat{\boldsymbol{q}}(\omega)$ is the non-trivial kernel of $\Phi(\omega)$, the general solution is

$$\hat{\boldsymbol{u}}_1(\tau_1; \omega) = \hat{B}(\tau_1; \omega)\hat{\boldsymbol{q}}(\omega), \tag{3.3}$$

with $\hat{B}$ a slowly varying complex scalar amplitude to be determined. At order $O(\epsilon_o^2)$, we obtain

$$\Phi\hat{\boldsymbol{u}}_2 = -\hat{\boldsymbol{q}}\mathrm{d}_{\tau_1}\hat{B} + \hat{\boldsymbol{g}}_2[\hat{B}] + \phi\boldsymbol{f}_h\hat{\xi} - \boldsymbol{f}_o\hat{B}, \tag{3.4}$$

for which we have used that $P\hat{B}\hat{\boldsymbol{q}} = \hat{B}\boldsymbol{f}_o$ and defined $\hat{\boldsymbol{g}}_2[\hat{B}] \doteq \mathcal{F}[N_2(\mathcal{F}^{-1}[\hat{B}\hat{\boldsymbol{q}}])]$.

Note that because the slow time scales as ϵ_o, the term $\hat{\boldsymbol{q}}\mathrm{d}_{\tau_1}\hat{B}$ and the term $\hat{\boldsymbol{g}}_2[\hat{B}]$, which compute the nonlinear interaction of the $O(\epsilon_o)$ solution with itself, appear at the same order in (3.4). Therefore, the slow time scale can be physically interpreted as the time scale at which the (weak) nonlinearities are influential. The operator Φ being singular, the only way for (3.4) to yield a non-diverging solution and thus preserve the asymptotic hierarchy is if the right-hand side is orthogonal to $\hat{\boldsymbol{a}}$, the kernel of $\Phi^\dagger$. This solvability condition (or Fredholm alternative) yields an amplitude equation for $\mathrm{d}_{\tau_1}\hat{B}$,

$$\{\hat{\boldsymbol{a}}, \hat{\boldsymbol{q}}\}\mathrm{d}_{\tau_1}\hat{B} = \hat{g}_2[\hat{B}] + \{\hat{\boldsymbol{a}}, \boldsymbol{f}_h\}\phi\hat{\xi} - \{\hat{\boldsymbol{a}}, \boldsymbol{f}_o\}\hat{B}, \tag{3.5}$$

where we have defined the functional $\hat{g}_2[\hat{B}] \doteq \{\hat{\boldsymbol{a}}, \hat{\boldsymbol{g}}_2[\hat{B}]\}$.

If $\hat{\boldsymbol{f}}_2$ designates the right-hand side of (3.4), the solvability condition $0 = \{\hat{\boldsymbol{f}}_2, \hat{\boldsymbol{a}}\} = \{R\hat{\boldsymbol{f}}_2, \hat{\boldsymbol{q}}\}$ implies $\hat{\boldsymbol{u}}_2 = R\hat{\boldsymbol{f}}_2$ to be directly the particular solution; by defining $\boldsymbol{u}_2(t) \doteq \mathcal{F}^{-1}[\hat{\boldsymbol{u}}_2]$, one can easily show that the solvability condition also implies that

$$\overline{\{\boldsymbol{u}_2(t), \boldsymbol{l}(t-\tau)\}} = \frac{1}{2\pi}\int_{-\infty}^{\infty}\hat{\xi}\{\hat{\boldsymbol{f}}_2, \hat{\boldsymbol{a}}\}\mathrm{e}^{-\mathrm{i}\tau\omega}\,\mathrm{d}\omega = 0, \quad \text{for all } \tau. \tag{3.6}$$

In words, a physical implication of the solvability condition is that, on average in the temporal domain, the second-order field must not project on the optimal response (which exhibits the largest possible maintained variance) or on any of its time-shifted versions. This preserves the asymptotic hierarchy, thereby guaranteeing that the expansion is well-posed.

We will refer to (3.5) as the Weakly Nonlinear Non-normal stochastic (WNNs) model. Depending, for instance, on the nature of the nonlinearity, it may already capture dominant weakly nonlinear effects, without the need for higher-order correction. This will be the case of our first application case, and in this scenario an equilibrium solution is found by solving (3.5) for a statistically steady regime $\mathrm{d}_{\tau_1}\hat{B} = 0$. In any case, and by definition, an equilibrium solution $\hat{B}(\omega)$ does not depend on the slow time scale(s) and is associated with the weakly nonlinear stochastic gain $G_{WNNs} = \overline{\langle||\epsilon_o\boldsymbol{u}_1(t)||^2\rangle}/F^2$, where the overline denotes the temporal average $\bar{\boldsymbol{u}} = T^{-1}\int_0^T \boldsymbol{u}\,\mathrm{d}t$. We can show that this is equivalent to

$$G_{WNNs} = \frac{1}{2\pi\epsilon_o^2\phi^2}\int_{-\infty}^{\infty}\langle|\hat{B}(\omega)|^2\rangle||\hat{\boldsymbol{q}}(\omega)||^2\,\mathrm{d}\omega. \tag{3.7}$$

The property $\overline{\mathrm{e}^{\mathrm{i}t(s-\omega)}} = 2\pi\delta(s-\omega)/T$ has been used in (3.7) to express the gain as a simple integral over the frequencies. Note that, by construction, $(2\pi)^{-1}\int_{-\infty}^{\infty}||\hat{\boldsymbol{q}}(\omega)||^2\,\mathrm{d}\omega = 1$.

Note that, in the time-independent case $\mathrm{d}_{\tau_1}\hat{B} = 0$, the method presented in this paper is in a certain sense more general than the method of harmonic balance, but in another sense more restricted. More general because the nonlinear evolution captured by the amplitude equation does not rely on the assumption that the dominant nonlinear mechanism is the Reynolds stress feedback onto the mean flow, thus does not neglect the nonlinearity arising from the cross-coupling between different frequencies. These cross-couplings are fully embedded in the term $\hat{g}_2[\hat{B}]$. More restricted, however, because our method explicitly relies on an asymptotic expansion, which makes it simpler to implement but in principle also limits its validity to weak forcing. This is not the case for the harmonic balance technique, which has been shown to work also in the strongly nonlinear regime, where the spatial

structure of the saturated response differs considerably from that of the linear regime (Mantic-Lugo & Gallaire 2016). Specifically, the harmonic balance technique typically retains the spatial degrees of freedom, whereas the space-independent amplitude equation condemns the response to be structurally close to the linear one.

In the linear regime $\phi \to 0$, the equilibrium solution of (3.5) is simply $\hat{B} = \phi\hat{\xi}\{\hat{\boldsymbol{a}}, \boldsymbol{f}_h\}/\{\hat{\boldsymbol{a}}, \boldsymbol{f}_o\}$. We can show that this implies $\langle\{\boldsymbol{u}_1(t), \boldsymbol{l}(t)\}\rangle = \phi\epsilon_o^2\{\boldsymbol{f}_h, B^\infty \boldsymbol{f}_o\} = \phi\{\boldsymbol{f}_h, \boldsymbol{f}_o\}$; therefore, if the applied forcing is orthogonal to $\boldsymbol{f}_o$, the response to the former will be *on average* orthogonal to the response of the latter, which is consistent. Conversely, if the optimal forcing is applied, the linear solution is $\hat{B} = \phi\hat{\xi}$ and leads to the expected gain $G = 1/\epsilon_o^2$. In the rest of this paper, we choose $\boldsymbol{f}_h = \boldsymbol{f}_o$ for the sake of simplicity.

The weakly nonlinear gain defined in (3.7) will be compared with the fully nonlinear gain extracted from a DNS of (2.1), and defined hereafter as

$$G_{DNS} \doteq \frac{\overline{\langle||\boldsymbol{u}_p(t)||^2\rangle}}{F^2} = \frac{1}{2\pi F^2}\int_{-\infty}^{\infty} ||\hat{\boldsymbol{u}}_p(\omega)||^2 \,\mathrm{d}\omega, \quad \text{with } \boldsymbol{u}_p(t) = \boldsymbol{U}(t) - \bar{\boldsymbol{U}}. \tag{3.8}$$

In contrast to the WNNs approach, the DNS are performed in the time domain for $t \in [0, T]$.

We first discuss the performance of the WNNs model on a toy model, for which our results should be easily reproducible. We consider the 2×2 system

$$\frac{\mathrm{d}\boldsymbol{U}}{\mathrm{d}t} = \boldsymbol{L}\boldsymbol{U} + ||\boldsymbol{U}||\boldsymbol{M}\boldsymbol{U} + F\xi(t)\boldsymbol{f}_o, \quad \text{with } \boldsymbol{L} = \begin{bmatrix} -1/Re & 1 \\ 0 & -2/Re \end{bmatrix}, \quad \boldsymbol{M} = \begin{bmatrix} 0 & -1 \\ -1 & 0 \end{bmatrix}; \tag{3.9}$$

thus the nonlinear operator in (2.1) is $N(\boldsymbol{U}) = \boldsymbol{L}\boldsymbol{U} + ||\boldsymbol{U}||\boldsymbol{M}\boldsymbol{U}$. This system is a slightly modified version of that in Trefethen *et al.* (1993) (where $M_{21} = 1$), such that its only stable equilibrium solution is $\boldsymbol{U}_e = \boldsymbol{0}$ (two other equilibria exist but are unstable).

Provided $Re \gg 1$, the matrix $\boldsymbol{L}$ is strongly non-normal and amplifies energy transiently, although its two eigenvalues $-1/Re$ and $-2/Re$ are strictly stable. For $Re = 160$ we compute $\boldsymbol{f}_o = [0.0125, 0.9999]^{\mathrm{T}}$ associated with the gain $1/\epsilon_o^2 = 3.4143 \times 10^5$. We solve the WNNs model numerically, with the amplitude equation (3.5) for $\mathrm{d}_{\tau_1}\hat{B} = 0$ uniformly discretised with N frequencies $\omega \in [0, \omega_c]$, where $\omega_c = 0.625$. More details are provided in the supplementary material § 1 available at https://doi.org/10.1017/jfm.2022.902.

In figure 1, predictions from the WNNs model are compared with fully nonlinear gains, where $\boldsymbol{U}(t)$ is extracted from a DNS of (3.9), for $t \in [0, T]$, with $T = 6.6 \times 10^5$ simulated and sampled at $\Delta t = \pi/\omega_c \approx 5$. For both the WNNs and the DNS approaches, the results have been ensemble-averaged over 10^4 realisations of the white noise. The agreement is remarkable for all the considered forcing amplitudes; thus we need not correct the amplitude equation with $O(\epsilon_o^3)$ terms. The WNNs model correctly predicts the monotonic decrease of the gain with the forcing amplitude (figure 1*a*) and the modification of the frequency distribution (figure 1*b*), in particular the significant increase of the most amplified frequency. We propose a tentative explanation for the shift of the response peak to higher frequencies in Appendix A. We have also verified that the predictions for the stochastic gain (see inset in figure 1*a*) and the Fourier spectra (not shown) remain very good for different values of the small parameter ϵ_o, namely for $Re = 20$ and $Re = 1280$.

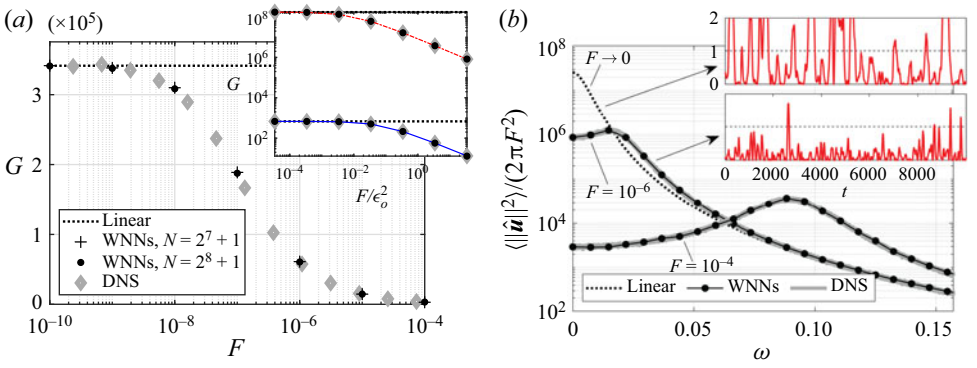

Figure 1. (*a*) Weakly and fully nonlinear stochastic gains (defined respectively in (3.7) and (3.8)) for the toy model (3.9), $Re = 160$. Inset: same for $Re = 20$ (continuous blue line) and $Re = 1280$ (dash-dotted red line), but in log–log scale and with the x-axis rescaled by the linear gain. (*b*) For the case $Re = 160$, associated ensemble-averaged Fourier spectra of the response $\hat{\boldsymbol{u}}$ (where $\epsilon_o\hat{\boldsymbol{u}}_1 = \epsilon_o\hat{B}\hat{\boldsymbol{q}}$ in the WNNs approach and $\hat{\boldsymbol{u}}_p$ in the DNS), normalised such that G is twice the area under the curve. Insets: single realisations of $\epsilon_o^2||\boldsymbol{u}_p(t)||^2/F^2$ as a function of time in the statistically steady regime (red solid line), and ensemble average in the linear regime (black dashed line).

3.2. *Bilinear system and application to the backward-facing step flow*

The weakly nonlinear evolution of the stochastic gain is now sought for the incompressible NSE. The nonlinear term $C(\boldsymbol{U}, \boldsymbol{U})$, where $C(\boldsymbol{a}, \boldsymbol{b}) \doteq ((\boldsymbol{b} \cdot \boldsymbol{\nabla})\boldsymbol{a} + (\boldsymbol{a} \cdot \boldsymbol{\nabla})\boldsymbol{b})/2$, is bilinear. Therefore, we expect essential nonlinear interactions to arise at third order in the expansion parameter, which we want to account for in the amplitude equation. Although it is certainly possible to correct (3.5) at order $O(\epsilon_o^3)$ after introducing a slower time scale τ_2, it is simpler to rescale the forcing and the linear term such that they appear directly at the third order. In this manner, we avoid a response at second order, which would interact at the next order and obscure the amplitude equation unnecessarily.

We propose the rescaled multiple-scale expansion

$$\boldsymbol{U}(t, \tau_1, \tau_2) = \boldsymbol{U}_e + \sqrt{\epsilon_o}\boldsymbol{u}_1(t, \tau_1, \tau_2) + \epsilon_o\boldsymbol{u}_2(t, \tau_1, \tau_2) + \sqrt{\epsilon_o}^3\boldsymbol{u}_3(t, \tau_1, \tau_2) + O(\epsilon_o^2), \tag{3.10}$$

where $\tau_1 = \sqrt{\epsilon_o}t$ and $\tau_2 = \epsilon_o t$. The flow is weakly forced by $\boldsymbol{F} = \phi\sqrt{\epsilon_o}^3\boldsymbol{f}_o\xi(t)$ (a second advantage of the rescaling is that the forcing amplitude $F = \phi\sqrt{\epsilon_o}^3$ is larger than that previously defined by a factor $1/\sqrt{\epsilon_o}$). Following the method outlined in the previous section, we introduce (3.10) in the NSE, take the Fourier component at ω and perturb the inverse resolvent according to (2.9). The solution at $O(\sqrt{\epsilon_o})$ is again $\hat{\boldsymbol{u}}_1(\tau_1, \tau_2; \omega) = \hat{B}(\tau_1, \tau_2; \omega)\hat{\boldsymbol{q}}(\omega)$. At order $O(\epsilon_o)$ we obtain

$$\Phi\hat{\boldsymbol{u}}_2 = -\hat{\boldsymbol{q}}\partial_{\tau_1}\hat{B} + \hat{\boldsymbol{g}}_2[\hat{B}], \tag{3.11}$$

with $\hat{\boldsymbol{g}}_2[\hat{B}] = -\mathcal{F}[C(\mathcal{F}^{-1}[\hat{B}\hat{\boldsymbol{q}}], \mathcal{F}^{-1}[\hat{B}\hat{\boldsymbol{q}}])]$. Imposing the Fredholm alternative such that the right-hand side ($\doteq \hat{\boldsymbol{f}}_2$) of (3.11) is orthogonal to $\hat{\boldsymbol{a}}$ yields $\{\hat{\boldsymbol{a}}, \hat{\boldsymbol{q}}\}\partial_{\tau_1}\hat{B} = \{\hat{\boldsymbol{a}}, \hat{\boldsymbol{g}}_2[\hat{B}]\} = \hat{g}_2[\hat{B}]$. The field $\hat{\boldsymbol{u}}_2^\perp \doteq R\hat{\boldsymbol{f}}_2$ is such that $\{\hat{\boldsymbol{u}}_2^\perp, \hat{\boldsymbol{q}}\} = \{\hat{\boldsymbol{f}}_2, \hat{\boldsymbol{a}}\} = 0$; thus $\Phi\hat{\boldsymbol{u}}_2^\perp = R^{-1}\hat{\boldsymbol{u}}_2^\perp$ and $\hat{\boldsymbol{u}}_2^\perp$ constitutes the particular solution of (3.11). The general solution can be written as $\hat{\boldsymbol{u}}_2 = \hat{\boldsymbol{u}}_2^\perp + \hat{B}_2\hat{\boldsymbol{q}}$, with an arbitrary component $\hat{B}_2\hat{\boldsymbol{q}}$ on the kernel. We set $\hat{B}_2 = 0$ in the following, such that the component on $\hat{\boldsymbol{q}}$ of the overall response is fully embedded in $\hat{B}$,

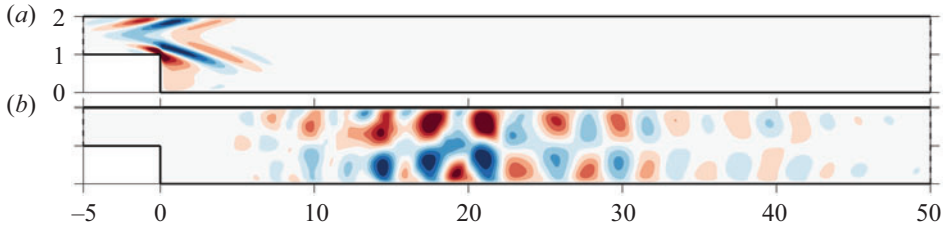

Figure 2. (*a*) Streamwise component of the optimal stochastic forcing $\boldsymbol{f}_o$ in the BFS flow, $Re = 500$. (*b*) DNS snapshot of the associated streamwise velocity response (around the base flow) for $F = 0.00025$.

which can be corrected at higher order thanks to its dependence on slower time scales. Consequently,

$$\hat{\boldsymbol{u}}_2[\hat{B}] = \hat{\boldsymbol{u}}_2^{\perp}[\hat{B}] = R(\hat{\boldsymbol{g}}_2[\hat{B}] - \{\hat{\boldsymbol{a}}, \hat{\boldsymbol{q}}\}^{-1}\hat{g}_2[\hat{B}]\hat{\boldsymbol{q}}). \tag{3.12}$$

Collecting terms at $O(\sqrt{\epsilon_o}^3)$, injecting the expressions for $\hat{\boldsymbol{u}}_1$ and $\hat{\boldsymbol{u}}_2$ and using the Fredholm alternative leads to an expression for $\partial_{\tau_2}\hat{B}$,

$$\{\hat{\boldsymbol{a}}, \hat{\boldsymbol{q}}\}\partial_{\tau_2}\hat{B} = \{\hat{\boldsymbol{a}}, \boldsymbol{f}_o\}(\phi\hat{\xi} - \hat{B}) - \{\hat{\boldsymbol{a}}, \partial_{\tau_1}\hat{\boldsymbol{u}}_2[\hat{B}]\} + \hat{g}_3[\hat{B}], \tag{3.13}$$

with the functional $\hat{g}_3[\hat{B}] = -\{\hat{\boldsymbol{a}}, \mathcal{F}[2C(\mathcal{F}^{-1}[\hat{B}\hat{\boldsymbol{q}}], \mathcal{F}^{-1}[\hat{\boldsymbol{u}}_2[\hat{B}]])]\}$. The *total* slow temporal evolution of $\hat{B}$ for a given frequency is found by combining partial derivatives with respect to the slow time scales (Orchini, Rigas & Juniper 2016) as $\mathrm{d}_{\tau_1}\hat{B} = \partial_{\tau_1}\hat{B} + (\partial_{\tau_1}/\partial_{\tau_2})\partial_{\tau_2}\hat{B} = \partial_{\tau_1}\hat{B} + \sqrt{\epsilon_o}\partial_{\tau_2}\hat{B}$. Eventually, it leads to leads to an ordinary differential equation for $\hat{B}$ (remember that $\boldsymbol{f}_h = \boldsymbol{f}_o$):

$$\{\hat{\boldsymbol{a}}, \hat{\boldsymbol{q}}\}\mathrm{d}_{\tau_1}\hat{B} = \hat{g}_2[\hat{B}] + \sqrt{\epsilon_o}[\{\hat{\boldsymbol{a}}, \boldsymbol{f}_o\}(\phi\hat{\xi} - \hat{B}) + \hat{g}_3[\hat{B}] - \partial_{\tau_1}\{\hat{\boldsymbol{a}}, \hat{\boldsymbol{u}}_2[\hat{B}]\}]. \tag{3.14}$$

An equilibrium solution $\hat{B}(\omega)$ of (3.14) is sought for given choices of ϕ and phase distribution for $\hat{\xi}$. It is associated with the statistically steady stochastic gain (3.7). In the linear regime, $\phi \to 0$ and $\hat{B} \to \phi\xi$, so the gain reduces to $G = 1/\epsilon_o^2$ as expected. All the nonlinear terms such as $\hat{g}_2[\hat{B}]$, $\hat{g}_3[\hat{B}]$ and $\partial_{\tau_1}\{\hat{\boldsymbol{a}}, \hat{\boldsymbol{u}}_2[\hat{B}]\}$ are convolution integrals accounting for the nonlinear interactions between the Fourier modes. They can be discretised in the frequency domain as quadratic or cubic products of the Fourier components of $\hat{B}(\omega)$. Detailed expressions are given in the supplementary material § 2, together with an algorithm to solve for the equilibrium solution.

We now consider the weakly nonlinear evolution of the stochastic gain in the two-dimensional BFS flow at $Re = 500$. This flow clearly illustrates streamwise non-normality, as evidenced, for example, in Blackburn *et al.* (2008). A Poiseuille profile of unit centreline velocity is imposed at the inlet. The nonlinear and linearised NSE are solved with the finite element method (see details in the supplementary material § 3). Figure 2(*a*) shows the optimal stochastic forcing $\boldsymbol{f}_o$, which is remarkably similar to the *harmonic* forcing structure at the optimal frequency $\omega = 0.47$ determined via a resolvent analysis (Mantic-Lugo & Gallaire 2016); the harmonic gain being maximal at $\omega = 0.47$, the associated forcing structure is naturally favoured when maximising the stochastic gain. Figure 2(*b*) shows a DNS snapshot of the flow response to $F\xi(t)\boldsymbol{f}_o$ for $F = 0.00025$.

The results of the WNNs model are reported in figure 3, where the amplitude equation (3.14) for $\mathrm{d}_{\tau_1}\hat{B} = 0$ was uniformly discretised with N frequencies $\omega \in [0, \omega_c]$ with $\omega_c = \pi$, and the results were ensemble-averaged over 500 realisations of the white noise.

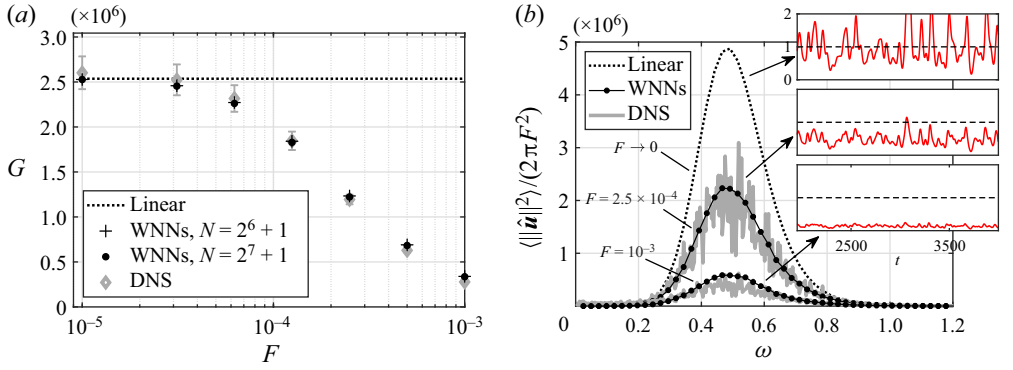

Figure 3. Same as figure 1 for the BFS flow, $Re = 500$. Error bars around DNS points show plus or minus one standard deviation.

Predictions from the DNS are also shown, resulting from simulations of duration $T = 2049$ after the transients fade away, sampled at $\Delta t = \pi/\omega_c = 1$ and ensemble-averaged over 10 realisations of the white noise (this lower number of realisations is the consequence of each one being numerically costly). Unlike the toy model of § 3.1, the amplitude equation built from a forcing introduced at second order and stopped at second order did not capture significant nonlinear effects (not shown). Introducing instead the forcing at third order, as described above, the comparison with DNS data is conclusive: the stochastic gains experience a monotonic decay with increasing F, also associated with a decreasing standard deviation for the DNS data.

We now emphasise that the fully nonlinear stochastic gain in (3.8) considers perturbation around the *temporal mean* flow, and not around the *base* flow $\boldsymbol{U}_e$. This distinction was unimportant in the previous application case since the nonlinearity did not generate a temporal mean. The creation of non-zero temporal mean ($\overline{\boldsymbol{U}(t)} \neq 0$) is associated with a diverging behaviour of the Fourier component at $\omega = 0$, as the normalisation in (2.4*a*,*b*) directly implies $\hat{\boldsymbol{U}}(0) = \overline{\boldsymbol{U}(t)}\sqrt{T} \to \infty$. Since this divergence is unlikely to be captured by $\hat{B}(0)$, we omitted its contribution in the gain calculation, but noted that this did not change the gain. However, the WNNs model certainly takes into account the effects of temporal mean flow corrections on $\hat{\boldsymbol{u}}_1(\omega)$, as such steady corrections are created at the next order and embedded in $\boldsymbol{u}_2(t)$.

For small F close to the linear regime, DNS and WNNs show some discrepancies (figure 3*a*) that are believed to be due to an imperfect convergence of the DNS data, because of the large standard deviation at small F and the limited number of realisations. The limit of large F is also associated with a slight departure of the (well-converged) DNS data from the WNNs predictions, although it is believed this time to be due solely to increasingly strong nonlinearities. In figure 3(*b*), the Fourier spectra reveal that increasing F conserves the most amplified frequency, which may be due to the fact that the forcing structure is fixed to $\boldsymbol{f}_o$, extremely similar to the optimal harmonic forcing for $\omega = 0.47$. In the inset, from the temporal evolution of the signal $\propto ||\boldsymbol{u}(t)||^2$ we recover that, for this particular flow, nonlinearities not only saturate the average level of energy of the response, but also significantly reduce the amplitude of the oscillations (i.e. the standard deviation).

Finally, note that the asymptotic expansions (3.1) and (3.10) have been scaled differently in order for the linear ($\propto \hat{B}$) and forcing ($\propto \phi\hat{\xi}$) terms to appear at the last considered order. This raises the question of how to know *a priori*, and for a given nonlinearity,

the minimal order that should be considered. Although a 'trial and error' process is always arguably acceptable, we postulate that it is the earliest order where the nonlinear term generates a component oscillating at ω_o, in the limit where the linear response $\hat{\boldsymbol{q}}$ is monochromatic and oscillating at ω_o. Indeed, if we impose the solvability condition solely at the order(s) before, $\hat{B}$ will conserve its linear value, for the nonlinear term will naturally yield a null scalar product with the adjoint for all frequencies (both fields being non-zero at different frequencies). This scenario, which we want to avoid, does not occur in the opposite limit where the frequency spectrum of $\hat{\boldsymbol{q}}$ is flat. Of course, the linear optimal response has generally no reason to be monochromatic, but might still show a maximum in energy at selective frequencies, as was the case in figures 1(*b*) and 3(*b*). If we express $\boldsymbol{u}_1 = \hat{B}\hat{\boldsymbol{q}}\mathrm{e}^{\mathrm{i}\omega_o t} + \text{c.c.}$, the nonlinearity of the toy system at second order (i.e. $||\boldsymbol{u}_1||\boldsymbol{M}\boldsymbol{u}_1$) already generates terms oscillating at ω_o; therefore it was sufficient to consider only up to this second order to see an improvement over the linear prediction. For the NSE, however, one needs to go to the third order to recover terms in ω_o (specifically $\hat{B}|\hat{B}|^2\mathrm{e}^{\mathrm{i}\omega_o t}$, as well known for classical weakly nonlinear equations for an eigenmode amplitude).

4. Conclusions

By generalising the method proposed in Ducimetière *et al.* (2022), we have derived an amplitude equation describing the weakly nonlinear, statistically steady response to stochastic forcing in arbitrarily stable yet non-normal systems. The amplitude depends solely on the frequency, and is therefore independent of the number of spatial degrees of freedom of the discretised system. This may save a significant amount of computational resources compared to fully nonlinear simulations, where long simulated times and/or many realisations are needed to ensure statistical convergence, which becomes rapidly impracticable for large systems like fluid flows. The amplitude equation has been successfully compared to fully nonlinear numerical simulations, and predicts well the variation of both the stochastic gain and the Fourier spectrum with the forcing amplitude.

Future research may include applying the method to realistic flows (e.g. atmospheric flows subject to weak forcing, such as zonal jets in barotropic flows (Bouchet, Nardini & Tangarife 2013)), and developing extensions towards systems with multiple attractors and noise-induced transition.

Supplementary material. Supplementary material is available at https://doi.org/10.1017/jfm.2022.902.

Acknowledgements. The authors would like to thank the anonymous referees for constructive questions and comments on the manuscript.

Funding. We acknowledge the Swiss National Science Foundation under grant 200341.

Declaration of interests. The authors report no conflict of interest.

Author ORCIDs.
Yves-Marie Ducimetière https://orcid.org/0000-0003-4018-5751;
Edouard Boujo https://orcid.org/0000-0002-4448-6140;
François Gallaire https://orcid.org/0000-0002-3029-1457.

Appendix A. Toy system: nonlinear upshift of the most amplified frequency

In figure 1(*b*), the peak of the linear response in $\omega = 0$ is due to the presence of both eigenvalues on the imaginary axis (although their location alone is insufficient to deduce

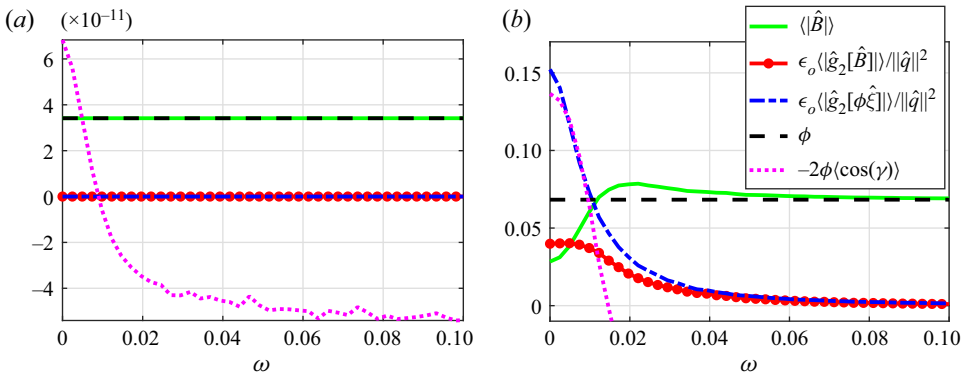

Figure 4. Ensemble averages: (*a*) $F = 10^{-16}$. (*b*) $F = 2 \times 10^{-7}$.

the stochastic gain, due to the non-normality of the operator). We explain the shift of the peak to higher frequencies with increasing nonlinearities as follows.

The equilibrium solution ($\mathrm{d}_{\tau_1}\hat{B} = 0$) of the amplitude equation (3.5) reads

$$\hat{B} = \epsilon_o ||\hat{\boldsymbol{q}}||^{-2} \hat{g}_2[\hat{B}] + \phi\hat{\xi}, \tag{A1}$$

where we used that $\{\hat{\boldsymbol{a}}, \boldsymbol{f}_o\} = \{\hat{\boldsymbol{q}}, \hat{\boldsymbol{q}}\}/\epsilon_o = ||\hat{\boldsymbol{q}}||^2/\epsilon_o$. We plot in figure 4 the ensemble average of the absolute values of: (1) the solution, $\langle|\hat{B}|\rangle$; (2) the nonlinear term, $\epsilon_o||\hat{\boldsymbol{q}}||^{-2}\langle|\hat{g}_2[\hat{B}]|\rangle$; (3) the same nonlinear term but replacing $\hat{B}$ by its solution in the linear regime $\phi\hat{\xi}$, i.e. $\epsilon_o||\hat{\boldsymbol{q}}||^{-2}\langle|\hat{g}_2[\phi\hat{\xi}]|\rangle$; and (4) the linear stochastic forcing term, $\langle|\phi\hat{\xi}|\rangle = \langle\phi\rangle = \phi$. In the linear regime for $F = 10^{-16}$ ($\phi \to 0$) in figure 4(*a*), $\hat{B} = \phi\hat{\xi}$ is the solution, for the nonlinear term $\hat{g}_2$ is virtually zero. However, when we increase the forcing up to $F = 2 \times 10^{-7}$ in figure 4(*b*), the nonlinear interaction of the linear (optimal) response $\phi\hat{\xi}\hat{\boldsymbol{q}}$ with itself is no longer negligible and creates a strong response peaked around $\omega = 0$, which projects back on the optimal response (see dash-dotted blue line in figure 4*b*). Thereby, $\hat{B} = \phi\hat{\xi}$ cannot be the solution any more, and $\hat{B}$ must adapt around $\omega = 0$ so as to enforce the solvability condition. In more physical terms, $\hat{B}$ must adapt around $\omega = 0$ such that the nonlinear interaction of $\hat{B}\hat{\boldsymbol{q}}$ with itself is less amplified around $\omega = 0$ than that of $\phi\hat{\xi}\hat{\boldsymbol{q}}$, thus preserving the asymptotic hierarchy.

This is indeed what we observe in figure 4(*b*), where the red curve (with the bullet markers) is significantly less amplified than the dashed blue one. Whether this new $\hat{B}$ must have a larger or smaller amplitude than its linear value ϕ is given by the phase difference, which we call γ, between the nonlinear and the forcing terms in (A1). It is easy to show that $|\hat{B}| \leqslant \phi$ if and only if

$$-2\phi\cos(\gamma) \geqslant \epsilon_o ||\hat{\boldsymbol{q}}||^{-2} |\hat{g}_2[\hat{B}]|. \tag{A2}$$

For this reason we show $-2\phi\langle\cos(\gamma)\rangle$ in figure 4(*b*) (see the magenta dotted line). In the range $0 \leqslant \omega \leqslant 0.012$, $\langle\cos(\gamma)\rangle$ decreases monotonically from -1 at $\omega = 0$ (the forcing and the nonlinear terms are in antiphase) to -0.2 at $\omega = 0.012$. In addition, the magenta dotted line is above the red one, thus $\langle|\hat{B}|\rangle \leqslant \phi$ and the nonlinearities are saturating in the sense that the weakly nonlinear response is of lower amplitude than the linear one. On the contrary, for $\omega \geqslant 0.012$ the phase difference between the forcing and the nonlinear terms

is such that $\langle|\hat{B}|\rangle \geqslant \phi$ and the nonlinearities are desaturating. Therefore, the maximum of $||\hat{B}\hat{\boldsymbol{q}}||$ is now increased to $\omega = 0.005$. This tendency is conserved for all the considered F.

References

Blackburn, H.M., Barkley, D. & Sherwin, S.J. 2008 Convective instability and transient growth in flow over a backward-facing step. *J. Fluid Mech.* **603**, 271–304.

Bouchet, F., Nardini, C. & Tangarife, T. 2013 Kinetic theory of jet dynamics in the stochastic barotropic and 2D Navier–Stokes equations. *J. Stat. Phys.* **153**, 572–625.

Dergham, G., Sipp, D. & Robinet, J.-Ch. 2013 Stochastic dynamics and model reduction of amplifier flows: the backward facing step flow. *J. Fluid Mech.* **719**, 406–430.

Ducimetière, Y.-M., Boujo, E. & Gallaire, F. 2022 Weak nonlinearity for strong non-normality. *J. Fluid Mech.* **947**, A43.

Farrel, B.F. & Ioannou, P.J. 2019 *Statistical State Dynamics: A New Perspective on Turbulence in Shear Flow*, pp. 380–400. Cambridge University Press.

Farrell, B.F. & Ioannou, P.J. 1993 Stochastic forcing of the linearized Navier–Stokes equations. *Phys. Fluids* A **5** (11), 2600–2609.

Farrell, B.F. & Ioannou, P.J. 1996 Generalized stability theory. Part I: autonomous operators. *J. Atmos. Sci.* **53** (14), 2025–2040.

Farrell, B.F. & Ioannou, P.J. 2003 Structural stability of turbulent jets. *J. Atmos. Sci.* **60** (17), 2101–2118.

Farrell, B.F. & Ioannou, P.J. 2012 Dynamics of streamwise rolls and streaks in turbulent wall-bounded shear flow. *J. Fluid Mech.* **708**, 149–196.

Garnaud, X., Lesshafft, L., Schmid, P.J. & Huerre, P. 2013 Modal and transient dynamics of jet flows. *Phys. Fluids* **25**, 044103.

Jovanović, M.R. & Bamieh, B. 2005 Component-wise energy amplification in channel flows. *J. Fluid Mech.* **534**, 145–183.

Mantic-Lugo, V. & Gallaire, F. 2016 Self-consistent model for the saturation mechanism of the response to harmonic forcing in the backward-facing step flow. *J. Fluid Mech.* **793**, 777–797.

Marston, J.B., Chini, G.P. & Tobias, S.M. 2016 Generalized quasilinear approximation: application to zonal jets. *Phys. Rev. Lett.* **116**, 214501.

Marston, J.B., Conover, E. & Schneider, T. 2008 Statistics of an unstable barotropic jet from a cumulant expansion. *J. Atmos. Sci.* **65** (6), 1955–1966.

McKeon, B.J. & Sharma, A.S. 2010 A critical-layer framework for turbulent pipe flow. *J. Fluid Mech.* **658**, 336–382.

Meliga, P. 2017 Harmonics generation and the mechanics of saturation in flow over an open cavity: a second-order self-consistent description. *J. Fluid Mech.* **826**, 503–521.

Nayfeh, A.H. & Serhan, S.J. 1990 Response statistics of non-linear systems to combined deterministic and random excitations. *Intl J. Non-Linear Mech.* **25** (5), 493–509.

Orchini, A., Rigas, G. & Juniper, M.P. 2016 Weakly nonlinear analysis of thermoacoustic bifurcations in the Rijke tube. *J. Fluid Mech.* **805**, 523–550.

Pickering, E., Rigas, G., Nogueira, P.A.S., Cavalieri, A.V.G., Schmidt, O.T. & Colonius, T. 2020 Lift-up, Kelvin–Helmholtz and Orr mechanisms in turbulent jets. *J. Fluid Mech.* **896**, A2.

Rajan, S. & Davies, H.G. 1988 Multiple time scaling of the response of a Duffing oscillator to narrow-band random excitation. *J. Sound Vib.* **123** (3), 497–506.

Rosenberg, K. & McKeon, B.J. 2019 Computing exact coherent states in channels starting from the laminar profile: a resolvent-based approach. *Phys. Rev.* E **100**, 021101.

Schmid, P.J. 2007 Nonmodal stability theory. *Annu. Rev. Fluid Mech.* **39** (1), 129–162.

Schmid, P.J. & Henningson, D. 2001 *Stability and Transition in Shear Flows*. Springer.

Symon, S., Rosenberg, K., Dawson, S.T.M. & McKeon, B.J. 2018 Non-normality and classification of amplification mechanisms in stability and resolvent analysis. *Phys. Rev. Fluids* **3**, 053902.

Tobias, S.M. & Marston, J.B. 2013 Direct statistical simulation of out-of-equilibrium jets. *Phys. Rev. Lett.* **110**, 104502.

Trefethen, L., Trefethen, A., Reddy, S. & Driscoll, T. 1993 Hydrodynamic stability without eigenvalues. *Science* **261**, 578–584.